

## Article

# Experimental Study and Visual Observation of a Loop Heat Pipe with a Flat Disk-Shaped Evaporator under Various Orientations

Huanfa Wang<sup>1</sup> , Guiping Lin<sup>1,2</sup>, Xiaobin Shen<sup>1,2,\*</sup> , Yong Liu<sup>3</sup> and Yuandong Guo<sup>1,2</sup>

<sup>1</sup> Laboratory of Fundamental Science on Ergonomics and Environmental Control, School of Aeronautic Science and Engineering, Beihang University, Beijing 100191, China; huanfawang@buaa.edu.cn (H.W.); gplin@buaa.edu.cn (G.L.); guoyd@buaa.edu.cn (Y.G.)

<sup>2</sup> Aircraft and Propulsion Laboratory, Ningbo Institute of Technology, Beihang University, Ningbo 315100, China

<sup>3</sup> Shenyang Aircraft Design & Research Institute, Shenyang 110035, China; liuyong@buaa.edu.cn

\* Correspondence: shenxiaobin@buaa.edu.cn; Tel.: +86-134-6658-4926

**Abstract:** In this study, visualization treatment was applied to the flat disk-shaped evaporator of a loop heat pipe. By observing the liquid/vapor behavior inside the evaporator and compensation chamber, the effects of orientation on the performances during startup and during a step-increase in heat load were investigated. With water as the working fluid, the loop heat pipe was tested under three typical orientations of  $\varphi = -90^\circ$ ,  $\varphi = 0^\circ$ , and  $\varphi = +90^\circ$ . The startup time was the shortest for the  $\varphi = -90^\circ$  orientation but there could be a slight temperature overshoot, resulting in an unsmoothed startup process. The startup speeds under the  $\varphi = 0^\circ$  and  $\varphi = +90^\circ$  orientations were similar, both without any significant temperature overshoot. The orientation could significantly change the heat leak and, therefore, the operating temperature and the heat-transfer limit. For the  $\varphi = +90^\circ$  and  $\varphi = -90^\circ$  orientations, the heat-transfer limits were about 71% and 157% of the value at the  $\varphi = 0^\circ$  orientation, respectively. Based on visual observations, for the loop heat pipe operating in gravity-driven mode, there could be two different paths for the working fluid to return to the evaporator, namely, along the vapor line for low heat loads and along the condenser and liquid lines for relatively large heat loads, respectively.

**Keywords:** loop heat pipe; flat disk-shaped evaporator; visual observation; orientation; gravity-driven mode



**Citation:** Wang, H.; Lin, G.; Shen, X.; Liu, Y.; Guo, Y. Experimental Study and Visual Observation of a Loop Heat Pipe with a Flat Disk-Shaped Evaporator under Various Orientations. *Energies* **2023**, *16*, 5068. <https://doi.org/10.3390/en16135068>

Academic Editor: Dmitry Eskin

Received: 14 May 2023

Revised: 20 June 2023

Accepted: 27 June 2023

Published: 30 June 2023



**Copyright:** © 2023 by the authors. Licensee MDPI, Basel, Switzerland. This article is an open access article distributed under the terms and conditions of the Creative Commons Attribution (CC BY) license (<https://creativecommons.org/licenses/by/4.0/>).

## 1. Introduction

With the rapid development of electronic technology, the heat generation and heat flux of electronics have also increased significantly. To solve the increasingly serious heat dissipation problems, multiple technology paths have been proposed and developed in recent years, such as the phase-change material heat sink [1–3], the microchannel heat sink [4,5], spray cooling [6–9], and the loop heat pipe (LHP) [10–12]. Among them, the LHP is a phase-change heat-transfer system with high heat-transfer efficiency and installation flexibility [13]. The capillary force generated spontaneously in the porous wick is the driving force that circulates the working fluid in the loop and no additional power input is required, resulting in high reliability. In consideration of the above advantages, the LHP technology is an important solution for the future of heat dissipation in electronics, such as CPU (Central Processing Unit), GPU (Graphics Processing Unit), and LED (Light Emitting Diode) [14,15]. The LHP consists primarily of an evaporator with a compensation chamber (CC), a condenser, and vapor and liquid lines [13,16]. The evaporator is the most critical component of a LHP and can be divided into cylindrical-type and flat-type from the shape [15]; the LHP with the flat evaporator, usually abbreviated as FLHP, can achieve lower contact thermal resistance and a more promising application value as a result of the shape

fitting with the common heat source. Until now, many different types of FLHP evaporators have been designed and developed, which can be divided into “opposite replenishment” type and “longitudinal replenishment” type according to the relative position of the CC and the heating surface [17]. Among them, the FLHP with the disk-shaped opposite replenishment evaporator is one of the important ones and has received some attention.

In the application of LHP technology in terrestrial environments, the influence of the installation orientation is an inevitable issue. However, for the FLHP with a disk-shaped evaporator, the related studies have been rather limited. Celata et al. [18] placed the evaporator and condenser of a disk-shaped FLHP at the same height and investigated the performances under two orientations, i.e., evaporator above the CC and evaporator below the CC. The test results showed that the orientation that had the evaporator located above the CC could lead to some temperature and hydraulic oscillations. Chen et al. [19] evaluated the thermal performance of a disk-shaped FLHP with tilts of  $0^\circ$  and  $18^\circ$ , where the condenser was set at the same height as the evaporator and 9.3 cm higher than the evaporator, respectively. The experimental results indicated that a tilt of  $18^\circ$  could shorten the startup time and reduce the thermal resistance. Maydanik et al. [15] positioned a disk-shaped LHP at the system slopes of  $\varphi = +90^\circ$  (evaporator on the top),  $\varphi = 0^\circ$  (evaporator at the same height as the condenser), and  $\varphi = -90^\circ$  (evaporator at the bottom) and found that the variation in the maximum heat-transfer limit would be no more than 20–25%. Maydanik et al. [14] also examined the effect of orientations on another disk-shaped FLHP and the maximum change in heat load was less than 30%. Wu et al. [20] studied a multi-evaporator FLHP with three disk-shaped evaporators in parallel; the results showed that the gravity-assisted angle could not only improve the steady state performance but could also speed up the startup process.

Visualization is an effective approach to obtaining the vapor and liquid behavior inside the system that can make up for the shortcomings of conventional measurements and deepen the understanding of the related physical mechanism. Until now, two main technologies, neutron radiography and direct observation, have been developed to achieve the visualization of LHPs.

Neutron radiography is a non-destructive method that has little effect on the heat/ mass transfer process due to the fact that the LHP structure has not been modified. As early as 2004, Cimbala et al. [21] verified the effectiveness of neutron radiography in the visual observation of an ammonia LHP. In that study, the relationship between the neutron images and the liquid/vapor distribution was established and some interesting phenomena, such as reverse flow and partial wick dry-out, were detected. Chuang et al. [22,23] proposed and confirmed the operating theory of a LHP operating under gravity-assisted orientation with the help of neutron radiography technology. Okamoto and Hatakenaka et al. [24,25] utilized neutron radiography to investigate the liquid behavior inside the evaporator of a miniature LHP at steady-state operation, as well as the dry-out of the primary wick during startup. Additionally, the effect of the secondary wick on the liquid/vapor distributions was also compared. Maydanik et al. [26] compared two LHPs, with ammonia and methanol as the working fluids, respectively, and discussed the effects of orientations and heat loads on the basis of neutron images. For the methanol LHP, oscillations of the liquid–vapor interface could be recorded clearly in the compensation chamber and the condenser.

However, neutron radiography manifests some disadvantages, such as inconvenient experiment construction and lack of detail. Therefore, the other visualization technology, direct observation through intrusive borescopes or transparent structures, has received greater application. The intrusive borescope is an effective tool to achieve the direct visualization of some container-like components, such as the compensation chamber and the liquid core. D’Entremont and Ochterbeck [27,28] designed a LHP with a cylindrical evaporator and a set of movable borescopes was inserted into the liquid core and compensation chamber. With the help of the borescopes, the vapor formation, movement, and distribution in the liquid core and compensation chamber during the LHP steady-state operation, startup, and deprime were observed and analyzed. Later, Chang et al. [29,30] ap-

plied the borescopes to visualization studies of the evaporator and compensation chamber of a two-evaporator-one-condenser LHP.

Other than the observation through borescopes, transforming the related components to be transparent is another technical solution. So far, only a few studies have utilized this technique to visualize LHPs to varying degrees. Among these studies, except for a few that dealt only with the visualization of LHP external loops, such as transport lines [31] and condensers [32–35], the majority were more concerned with the evaporator and CCs.

Regarding the visualization studies of cylindrical evaporator LHPs, some representative ones deserved to be reviewed below. Lin et al. [36] completed the partial-visualization of a dual compensation chamber loop heat pipe with the help of assembled glass windows. In this research, the authors described the bubble dynamics and liquid level in CCs with respect to the evaporator orientation; at the same time, the reverse flow in the condenser was also reported. By using a transparent tube as the casing for the evaporator and CC, Nishikawara et al. [37,38] observed the phase distribution and displacement inside the evaporator and established a link to LHP performance. Zhang et al. [39] realized the semi-sectional visualization of the cylindrical evaporator of a LHP. Based on the complete observation of bubble formation and liquid motion throughout the liquid core and CC, the phenomenon of temperature fluctuation was interpreted. Takamatsu et al. [40] visualized a cylindrical evaporator LHP, almost globally, and established the relationship between the bubble occupancy in the reverse region and LHP performance accordingly.

Except for the cylindrical evaporator LHP, the method of observing liquid/vapor behaviors through transparent structures was also applied to FLHPs. For a FLHP with a longitudinal replenishment evaporator, Bartuli et al. [41] reported a visualization scheme of the CC and the condenser and adopted similar ideas. Zhou et al. [42], Wang et al. [43], and Du et al. [44] further expanded the visualization scope to the vapor grooves. Aiming at the FLHP with a disk-shaped opposite replenishment evaporator, which is also the object of this paper, some visualization studies were also conducted. Mo et al. [45] investigated the temperature oscillations of a disk-shaped evaporator FLHP by using transparent materials to substitute the vapor/liquid line, condenser line, and part of the CC. Anand et al. [46] investigated the deprime process in the disk-shaped evaporator by visualizing the CC. Xu et al. [47,48] designed a FLHP with an optical disk-shaped evaporator of which the CC and vapor grooves could be observed. By means of this experimental setup, the effects of two-layer composite wicks and the working fluid inventory were studied in depth. Zhao et al. [49] developed a global visualization FLHP with a disk-shaped evaporator where the evaporator, the condenser, and the pipelines were all transparent. By observing the changes in liquid/vapor behavior, three startup stages were recorded and analyzed.

Based on the literature review above, with the help of the visualization study, the two-phase flow regime inside the FLHP has been widely observed and the understanding of the heat-transfer mechanisms has been gradually improved. However, to the best of the authors' knowledge, there have been few studies that have utilized visualization technology to investigate the effect of the orientation on the performance of a FLHP with a disk-shaped evaporator, resulting in a certain lack of clarity in terms of the operating mechanism. Therefore, in this study, the authors visualize the evaporator–CC assembly of a flat disk-shaped evaporator FLHP and observe the liquid/vapor behavior inside through the transparent structure. Through this visual observation, the effects of orientation on FLHP performances during startup, and during step increases in heat load, were analyzed and some new mechanisms were proposed, which could be helpful in promoting the terrestrial application of FLHPs.

## 2. Experimental Setup

### 2.1. Design and Description of the Visual FLHP

As displayed in Figure 1a, the object of this study was a set of visual FLHPs consisting of an evaporator, compensation chamber (CC), vapor line, liquid line, and condenser. The evaporator was disk-shaped and the CC was located opposite the heating surface of the

wick. To achieve the observation of the liquid and vapor behaviors, a visual design was applied to the evaporator–CC assembly. As presented in Figure 1b, the evaporator–CC assembly consisted primarily of the evaporator plate, the CC cover, the visualization window, and the capillary wick, all of which had been carefully designed to allow the system to be assembled and sealed properly. The evaporator plate and CC cover were both machined from brass and welded to the vapor line and liquid line, respectively. The active zone of the evaporator plate was circular, with a diameter of 50 mm; in addition, 12 parallel grooves, with both a width and a depth of 2 mm, were milled for vapor removal. The visualization window was made of quartz glass and annealed after flame polishing to obtain better optical properties and mechanical strength. The sealing of the evaporator–CC assembly was achieved by three fluoro-rubber O-rings, of which the deformation was created by the action of six bolts. The O-rings between the CC cover/evaporator plate and the visualization window provided the area of sealing between the working fluid in the evaporator–CC assembly and the external environment; meanwhile, the O-ring between the wick and the visualization window was used to prevent the vapor in the vapor grooves from directly entering the CC, which was also critical for the FLHP operation.

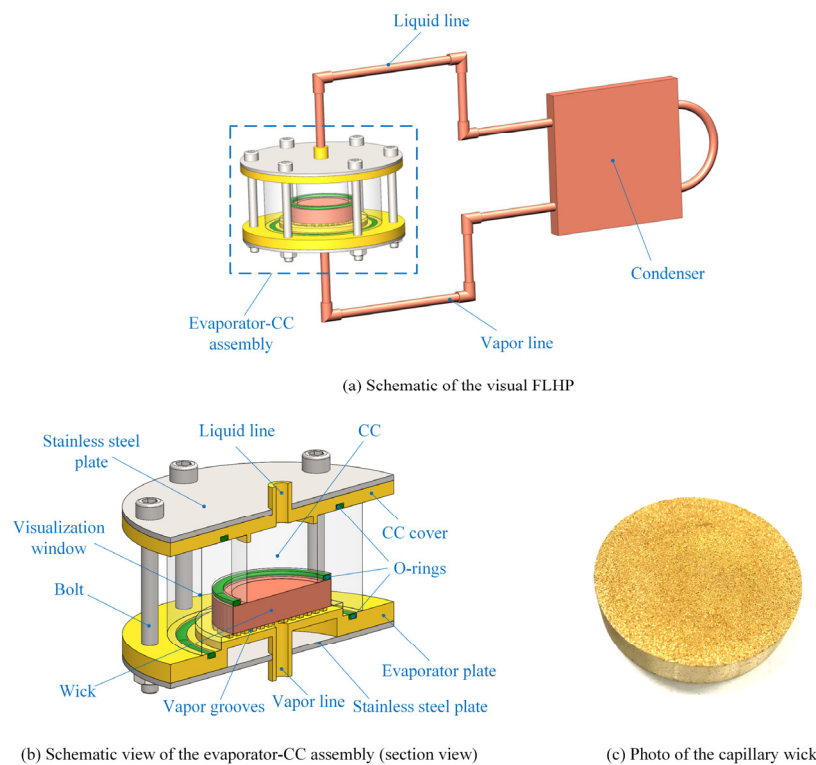


**Figure 1.** Description of the visual FLHP design.

The capillary wick (Figure 1c) was sintered by spherical copper powder. It was measured that the maximum equivalent diameter of the wick was  $44.76 \mu\text{m}$  and the porosity was 20.6%. The diameter of the wick was the same as the active zone of the evaporator plate (i.e., 50 mm) and the thickness was 10 mm. The interior of the CC was a cylindrical space with a diameter of 36 mm and a height of 25 mm; its internal volume could be calculated to be about 24.8 mL.

The vapor line and the liquid line were both circular copper tubes with an outer diameter of 6 mm, an inner diameter of 4 mm, and a length of 300 mm. The condenser was a copper coil heat exchanger with a channel diameter of 4 mm and an effective length of 294 mm; the condenser plate was measured to be  $100 \text{ mm} \times 100 \text{ mm} \times 10 \text{ mm}$ . In this study, water was selected as the working fluid and the filling volume was  $35 \pm 0.5 \text{ mL}$ , which was carefully designed and calculated to avoid operation failure.

## 2.2. Construction of the Experimental System

A schematic diagram of the experimental system is shown in Figure 2. The heat load was applied to the evaporator by an annular Kapton heater ( $\Phi 56/10$  mm) and its output power was controlled by a DC power supply (PSW 160-21.6, GW Instek, Taiwan, China). To reduce the heat leak to the environment, the Kapton heater was covered with aerogel felt, which was held in place with the help of a stainless steel plate. The condenser plate was cooled by an aluminum cold plate and the contact surface was filled with thermal grease to reduce the contact thermal resistance. The coolant for the cold plate was water at a temperature of  $5 \pm 0.1$  °C, which was provided and circulated by a cryostat.

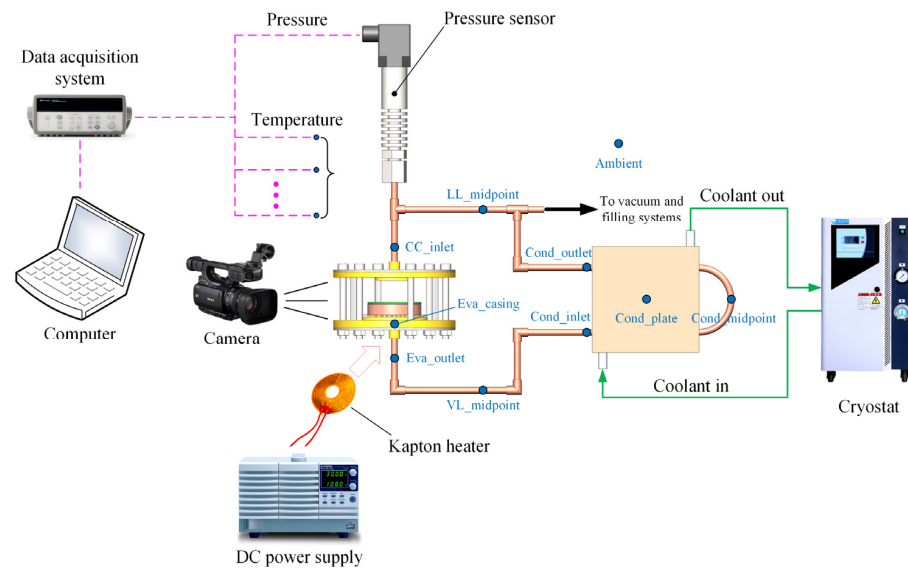


**Figure 2.** Schematic diagram of the experimental system.

The temperatures were measured by T-type thermocouples (TT-T-30, Omega Engineering, Norwalk, CT, USA), of which the measurement error was  $\pm 0.31$  °C. The arrangement of these thermocouples is marked in Figure 2. In addition, the pressure of the CC was also monitored by utilizing a pressure sensor with an accuracy of  $\pm 0.24\%$ . The temperature and pressure data were transformed by a set of data acquisition systems (34970A Data Acquisition/Switch Unit and 34901A Multiplexer Cards, Agilent Technologies, Santa Clara, CA, USA) and recorded by a computer. To capture the vapor-liquid distribution and movement within the evaporator–CC assembly, a high-resolution digital camera (XF105, Canon Inc., Tokyo, Japan) was employed. To reduce the heat exchange between the FLHP and the environment, all pipelines and condensers were wrapped in aerogel felt.

## 2.3. Description of the FLHP Orientations

The FLHP orientations studied in this paper are illustrated in Figure 3. In this work, the orientation in which the condenser and the evaporator–CC assembly were situated at the same height was selected as the reference orientation, i.e.,  $\varphi = 0^\circ$ , which was a general choice in the literature [15,19]. When the FLHP was placed at an orientation of  $\varphi = 0^\circ$ , the liquid line would be located above the vapor line, which could induce some gravity head. However, compared with the capillary force provided by the wick, the induced gravity head was relatively small and an orientation of  $\varphi = 0^\circ$  still could be considered a reference orientation. Based on the definition of the reference orientation and the coordinate, in the cases of  $\varphi = -90^\circ$  and  $+90^\circ$ , the positions of the condenser were above and below the evaporator–CC assembly, respectively. It should be noted that for the FLHP studied in this paper (flat evaporator with opposite replenishment), the liquid supply crisis should be avoided so that the CC should not be positioned approximately vertically below the evaporation area of the evaporator.

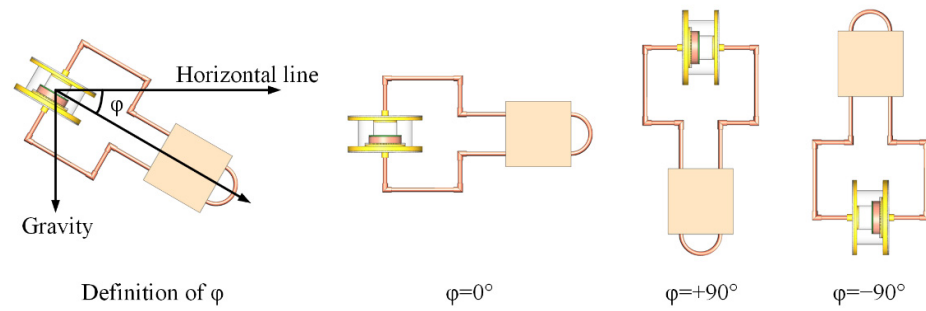


Figure 3. Definition of the FLHP orientation and three typical FLHP orientations.

### 3. Results and Discussion

The heat-transfer performance of a FLHP manifests rich connotations; in this paper, the temperature level, stability, and the heat-transfer limit of the designed visual FLHP during startup and a heat load increment test are discussed and analyzed emphatically.

#### 3.1. Startup Performances

##### 3.1.1. The Orientation of $\varphi = 0^\circ$

The startup process with a heat load of 30 W that was under an orientation of  $\varphi = 0^\circ$  is shown in Figure 4. It was obvious that the FLHP could start up and achieve a steady-state operation successfully. The increase in evaporator temperature could be taken as a sign of the beginning of heat load application. Almost simultaneously with the increase in temperature at the evaporator casing, the temperature at the evaporator outlet also increased due to heat conduction. After the evaporator was heated for about 3 min, a significant increase in CC pressure could be observed, which means that a temperature increase occurred in the CC and there was a large heat leak between the evaporator and the CC. The large heat leak could also be reflected in the visual observations. As shown in Figure 5, part of the vapor penetrated the wick into the CC directly, forming a violent heat/mass transfer process. In general, large heat leaks are usually unfavorable; they could result in high steady-state temperatures and even startup failure. As a result of the heat leak, the temperature of the CC inlet was also affected and rose considerably.

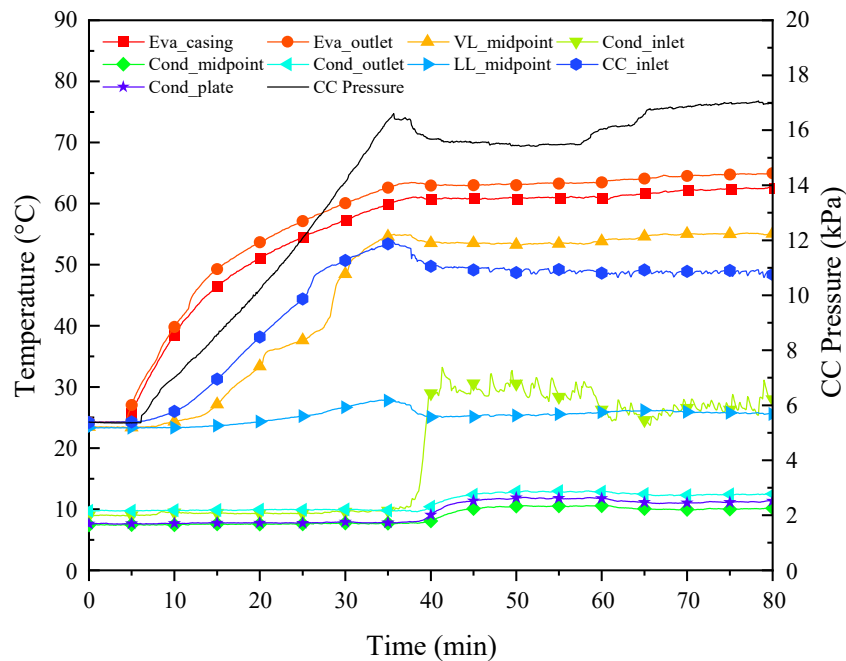
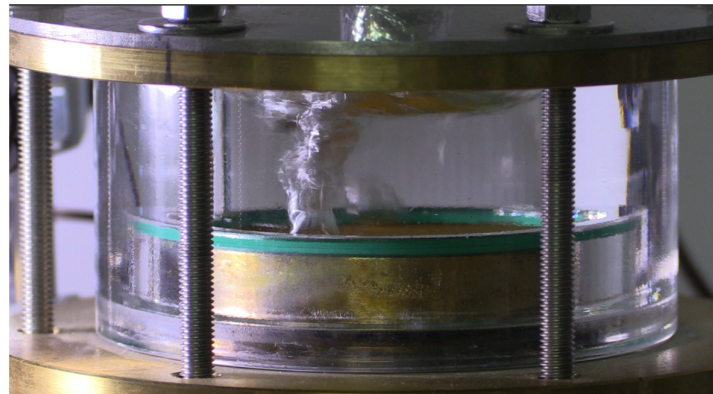


Figure 4. Startup process with a heat load of 30 W under an orientation of  $\varphi = 0^\circ$ .



**Figure 5.** Vapor penetrating the wick into the CC.

With the passage of heating time, the temperature of the vapor line increased gradually in the vapor flow direction. After the heat load was applied for about 8 min, the rise in temperature at the midpoint of the vapor line was monitored; for about 33 min, the temperature at the condenser inlet rose sharply, meaning that the vapor had arrived near the condenser. As the working fluid circulation was established, the liquid with a low temperature flowed into the CC, resulting in a mild decrease in the CC temperature and, therefore, the pressure.

Subsequently, the temperatures of the FLHP gradually evolved towards a steady state. Throughout the startup process, the evolution of the evaporator temperature was relatively smooth and the maximum evaporator temperature was basically consistent with that in the steady state; that is, there was no obvious temperature overshoot phenomenon (i.e., the operating temperature during the transient exceeded that in the steady state).

### 3.1.2. The Orientation of $\varphi = +90^\circ$

When the FLHP was adjusted to the  $\varphi = +90^\circ$  orientation, the temperature evolution during the startup, with a heat load of 30 W, was recorded, as shown in Figure 6. Regarding the overall viewpoint, the startup process was quite smooth and did not exhibit any temperature overshoot during this period. After the evaporator was heated, a gradual increase in the CC pressure could be observed almost simultaneously, which was more rapid than that of the  $\varphi = 0^\circ$  orientation. This could be attributed to the vertical orientation of the evaporator–CC assembly that allowed only part of the wick to reach the liquid with a low initial temperature in the CC, resulting in heat entering the CC more quickly. As a result of heat conduction, the temperature at the CC inlet also increased thereafter. The moment when the temperature rose at the midpoint of the vapor line could be monitored; it was 7 min after the heating of the evaporator, which was similar to the case  $\varphi = 0^\circ$ . Due to the low startup heat load and high working fluid circulation resistance, the vapor did not reach the condenser and, thus, no obvious temperature rise at the condenser inlet could be seen.

### 3.1.3. The Orientation of $\varphi = -90^\circ$

Compared to the other two orientations, the temperature evolution during the FLHP startup process under an orientation of  $\varphi = -90^\circ$  was not smooth enough and a slight temperature overshoot could be observed, as displayed in Figure 7. Similar to the case of  $\varphi = +90^\circ$ , the pressure rise in the CC also occurred simultaneously with the temperature rise in the evaporator, which also resulted from the fact that the wick was not being immersed completely by the liquid in the CC. The temperature rises at the midpoint of the vapor line and at the condenser inlet could be observed at 4 min and 6.8 min after the heat load was induced, respectively. After the vapor entered the condenser and the liquid entered the CC, a working fluid circulation was established and a temperature overshoot occurred after the heat load was applied for about 7.5 min. The maximum temperature at the evaporator

outlet was 41.7 °C during the overshoot, which was 3.0 °C higher than that in the steady state. The time required to establish a working fluid circulation was much shorter than in the other two cases, which might have been because the low circulation pressure benefited from the gravity-assisted attitude.

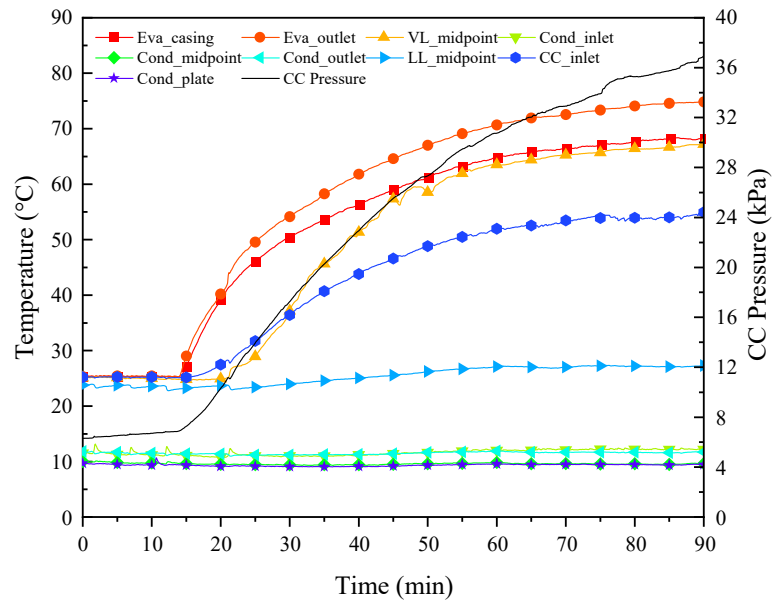


Figure 6. Startup process with a heat load of 30 W under an orientation of  $\varphi = +90^\circ$ .

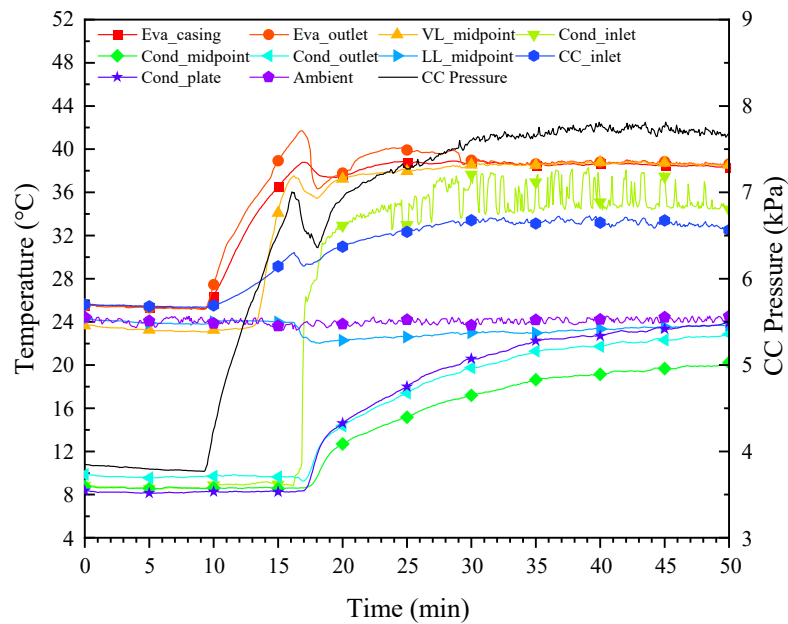


Figure 7. Startup process with a heat load of 30 W under an orientation of  $\varphi = -90^\circ$ .

### 3.2. Performances Analysis during the Step Increase in Heat Load

#### 3.2.1. The Orientation of $\varphi = 0^\circ$

Regarding when the FLHP was located at an orientation of  $\varphi = 0^\circ$ , the temperature and pressure evolutions during the step-increase in heat load are presented in Figure 8. During the test process, no significant temperature overshoot was observed in the evaporator. As the heat load increased step by step, the temperatures at the measurement points near the evaporator increased gradually. For safety considerations, the maximum heat load that the FLHP could operate stably at was 105 W; the evaporator temperature did not

exceed 110 °C. The temperature at the midpoint of the vapor line could be more reflective of the vapor temperature, which also increased gradually with the heat load. For the cases where the heat loads were 30 W and 105 W, the vapor temperatures were 55.1 °C and 60.8 °C, respectively. At a heat load of 30 W, the temperature at the condenser inlet was much lower than that at the midpoint of the vapor line and remained continuously fluctuating. This is because the condensation of the vapor had occurred before it entered the condenser as a result of the heat conduction from the condenser plate. As the heat load increased, the condenser inlet temperature began to rise gradually and finally reached the level of the vapor temperature in the vapor line at a heat load of 60 W, indicating that little condensation occurred before the vapor entered the condenser. When the heat load was 75 W, the temperature fluctuations at the condenser inlet disappeared, meaning that the vapor had entered the condenser completely.

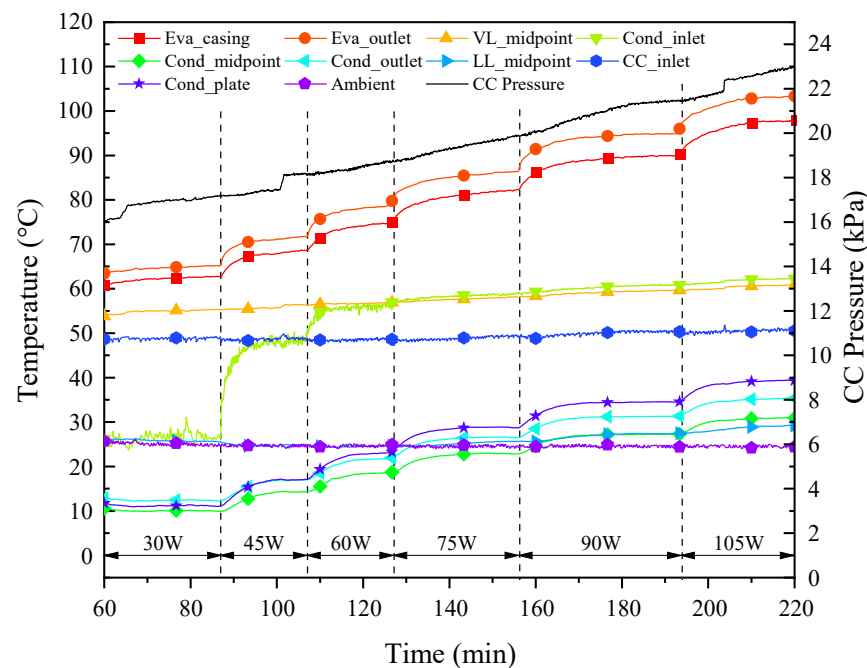


**Figure 8.** Temperature and pressure evolutions during the step increase in heat load under an orientation of  $\varphi = 0^\circ$ .

During the gradual increase of the heat load, the CC pressure showed slight sudden increases during the quasi-steady-state operation at heat loads of 30 W, 45 W, and 105 W. This phenomenon might have contributed to the change in the heat leak situation for some reason and resulted in a shift in the steady state of the system.

### 3.2.2. The Orientation of $\varphi = +90^\circ$

The temperature and pressure evolutions during the step increase of the heat load under an orientation of  $\varphi = +90^\circ$  are displayed in Figure 9, which shows little temperature overshoot. It could be seen that there was a considerable degradation in the FLHP performance compared to that of the  $\varphi = 0^\circ$  orientation. The heat-transfer limit of the FLHP within the allowable evaporator temperature (110 °C) was only 75 W, which was only about 71% of that under the  $\varphi = 0^\circ$  orientation. In addition, the temperature of the vapor in the vapor line ranged from 67.1 °C to 77.6 °C as the heat load increased from 30 W to 75 W, which was more than 10 °C higher than that under an orientation of  $\varphi = 0^\circ$ .

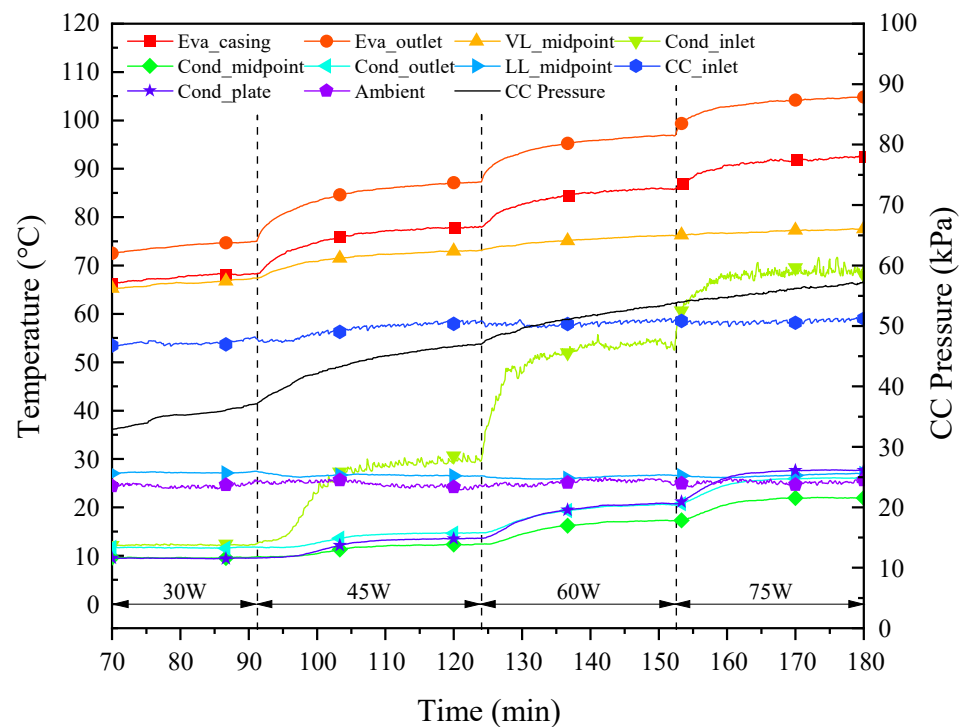
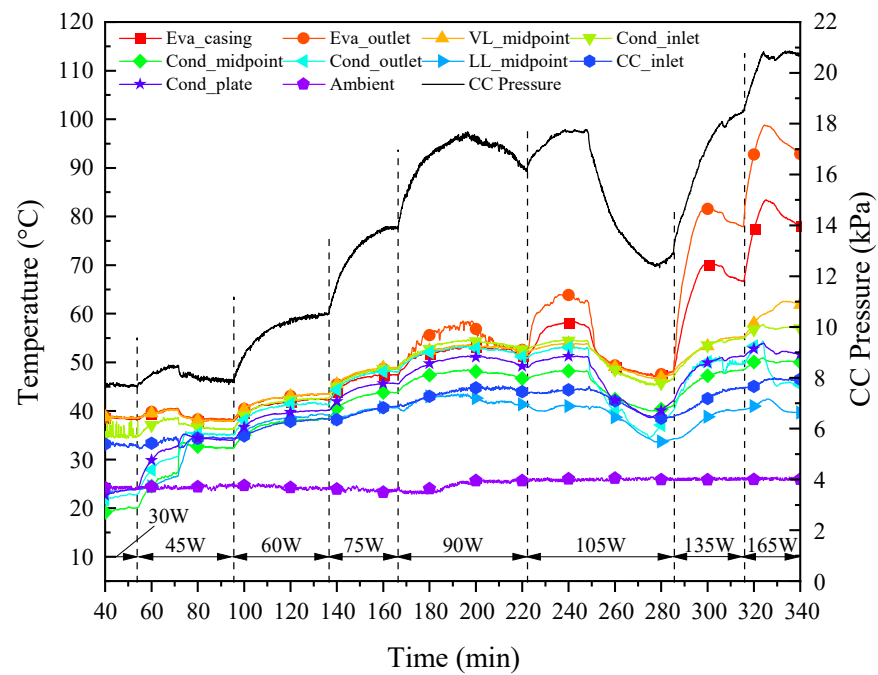


**Figure 9.** Temperature evolutions during the step increase in heat load under an orientation of  $\varphi = +90^\circ$ .

For the analysis at an orientation of  $\varphi = +90^\circ$ , the evaporator assembly was located above the condenser and the gravity acted as a resistance to the working fluid circulation. The additional resistance induced by gravity could enlarge the pressure difference between the evaporator and the CC, which, in turn, increased the heat leak and, therefore, the operating temperature. This was particularly prominent when water was chosen as the working fluid because the slope of its saturation pressure-temperature curve was quite small at low temperatures and a slight change in pressure could bring about a great change in temperature. As a result of the high heat leak and vapor temperature, the condensation phenomenon occurred primarily in the vapor line and led to a low temperature at the condenser inlet.

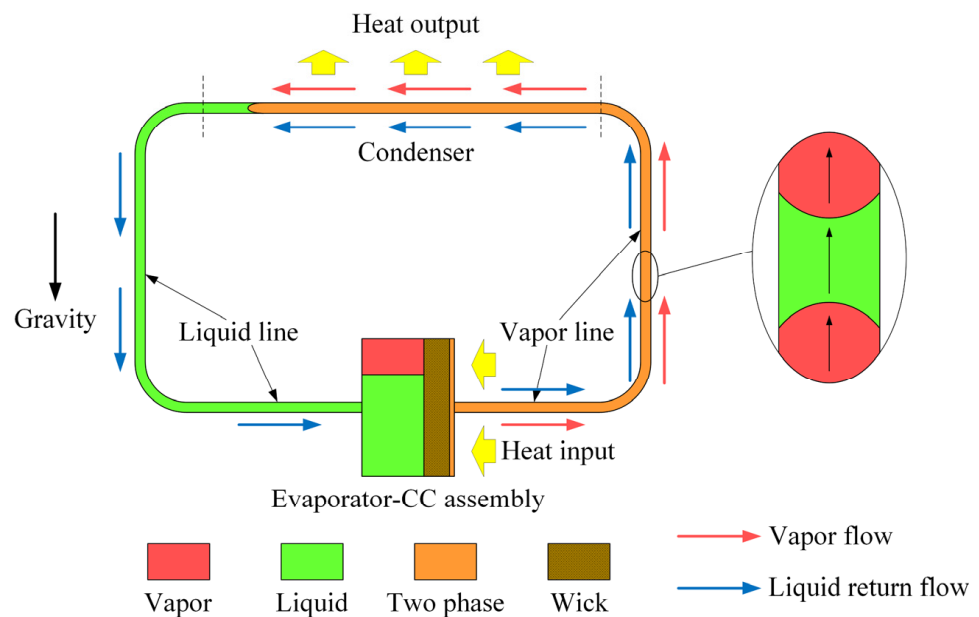
### 3.2.3. The Orientation of $\varphi = -90^\circ$

Figure 10 shows the temperature and pressure evolutions during the step increase in heat loads when the FLHP was situated at an orientation of  $\varphi = -90^\circ$ . On the premise that the evaporator temperature was not higher than  $110^\circ\text{C}$ , the maximum heat load was  $165\text{ W}$ , which was  $57\%$  higher than that of the  $\varphi = 0^\circ$  orientation. Compared to the other two orientations (i.e.,  $\varphi = 0^\circ$  and  $\varphi = +90^\circ$ ), the evaporator temperature exhibited more overshoots under an orientation of  $\varphi = -90^\circ$ ; for example, during the heat load increment from  $30\text{ W}$  to  $45\text{ W}$  and during the stepwise increase of the heat load from  $90\text{ W}$  to  $165\text{ W}$ . Throughout the augmentation of the heat load, the steady-state vapor temperature exhibited an “N-shaped” pattern of variation and the FLHP performances were much better than those at an orientation of  $\varphi = 0^\circ$ . During the heat load increment test, the vapor temperature would rise gradually over a heat load range of  $30\text{--}90\text{ W}$  and then experience some decrease as the heat load further increased to  $105\text{ W}$ . The vapor temperature would reach a peak at a heat load of  $90\text{ W}$ , of which the value was  $52.3^\circ\text{C}$ . After the heat load exceeded  $105\text{ W}$ , the vapor temperature increased again with the heat load, reaching a maximum of  $61.7^\circ\text{C}$  at a heat load of  $165\text{ W}$ .



**Figure 10.** Temperature and pressure evolutions during the step increase in heat load under an orientation of  $\varphi = -90^\circ$ .

Regarding the  $\varphi = -90^\circ$  orientation, the condenser was located above the evaporator-CC assembly, which was usually called the positive-elevation [22,23,50,51] or gravity-assisted attitude [30,52–54]. Under the circumstances, the general analysis determined that FLHP operation could be divided into gravity-driven mode and capillarity-gravity co-driven mode, depending on the value of the heat loads [22,23,50,52,54]. Regarding the operation of the gravity-driven mode, the circulation path of the working fluid is shown in Figure 11; the working fluid flow was driven entirely by the pressure gain from the liquid head between the liquid line and the vapor line.



**Figure 11.** General working fluid distribution and circulation path for gravity-driven mode.

Based on the flow path described in Figure 11, there should have been a returning liquid flow at the inlet of the CC when the operation of the FLHP was in gravity-driven

mode. However, the visual observation showed that there was no return liquid when the heat load was no more than 105 W, as shown in Figure 12, for example.

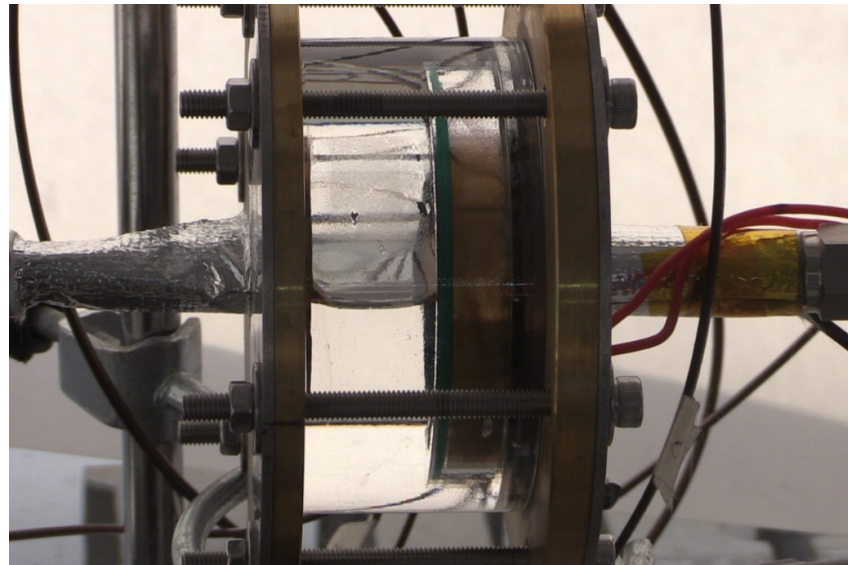


**Figure 12.** Liquid and vapor behavior under an orientation of  $\varphi = -90^\circ$  at a heat load of 105 W (no return liquid).

The inconsistency between the experimental phenomenon and the theory described in Figure 11 indicated that there seemed to be additional mechanisms in the operation theory of the LHP under gravity-assisted attitude. In fact, the theory described in Figure 11 was established under the assumption that the flow direction of condensate in the pipeline was exactly the same as that of the vapor. In general, this assumption was correct when the pipeline diameter was small enough, even at a low heat load (i.e., low vapor flow rate), and the effect of surface tension could enable the condensate in the condenser to be in a columnar shape and to be pushed forward by the vapor. However, with the expansion of the pipeline diameter, the surface tension would gradually fail to maintain the condensate being in a columnar shape and the condensate would be distributed in a film shape along the wall of the pipeline, forming an annular flow. At this time, if the heat load, and therefore the vapor flow rate, were not large enough, the condensation process would be dominated by gravity. Therefore, there could be another working fluid circulation path for a LHP operating under so-called “gravity-assisted attitude”, as shown in Figure 13. The vapor generated in the evaporator could be condensed gradually in an upward flow in the vapor line; the condensate would flow back to the evaporator directly in the form of a liquid film along the wall of the vapor line under the action of gravity, instead of flowing back to the CC through the condenser and the liquid line.

Compared to the liquid return path described in Figure 11, the other path described in Figure 13 clearly possessed a much smaller flow resistance. Therefore, when the heat load was relatively small, the low vapor flow rate could not prevent the condensate from returning to the evaporator along the inner wall of the vapor line by gravity, leaving the vapor line in a two-phase state. At this point, the working fluid flow in the vapor line was similar to that of the gravity heat pipe; therefore, it could be noted that for the case where the heat load was no more than 90 W, the evaporator and the vapor line manifested good temperature homogeneity, as shown in Figure 10.

When the heat load was increased to 105 W, the increase in vapor flow rate brought about a shear force large enough to prevent the condensate from flowing back along the inner wall of the vapor line; the return of the condensate would proceed through the path described in Figure 13, which was the classical “gravity driven” theory for LHPs. This can be corroborated by the visual observations shown in Figure 14, where an apparent liquid

return phenomenon can be seen at the CC inlet. Accompanied by the cold condensate passing through the liquid line and entering the CC, the pressure of the CC dropped significantly alongside that of the vapor temperature, as presented in Figure 10. At this time, the working fluid in the vapor line was still in a two-phase state; the liquid was entrained by the vapor and they flowed together towards the condenser so that the temperature at each position of the vapor line was almost the same and there was little superheating observed at the evaporator outlet.

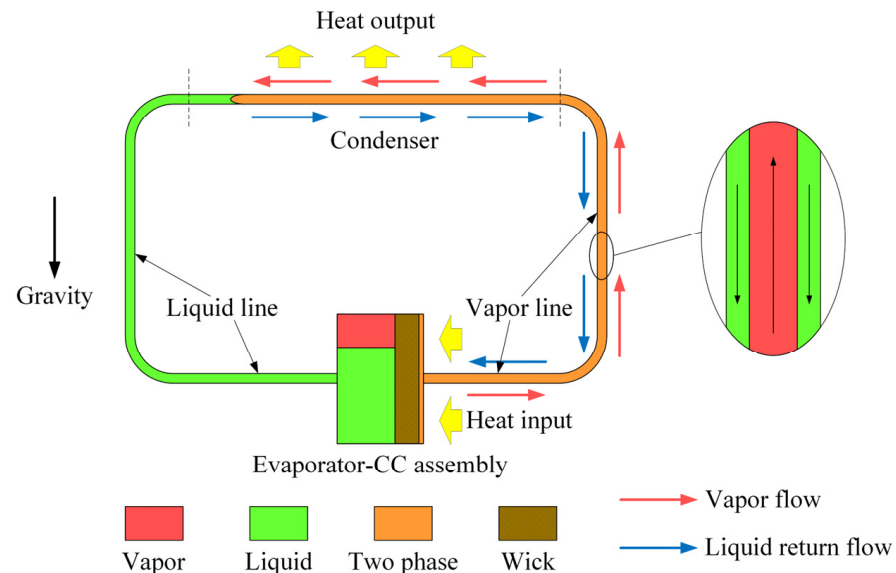


**Figure 13.** Another working fluid distribution and circulation path for the gravity-driven mode proposed in this study.

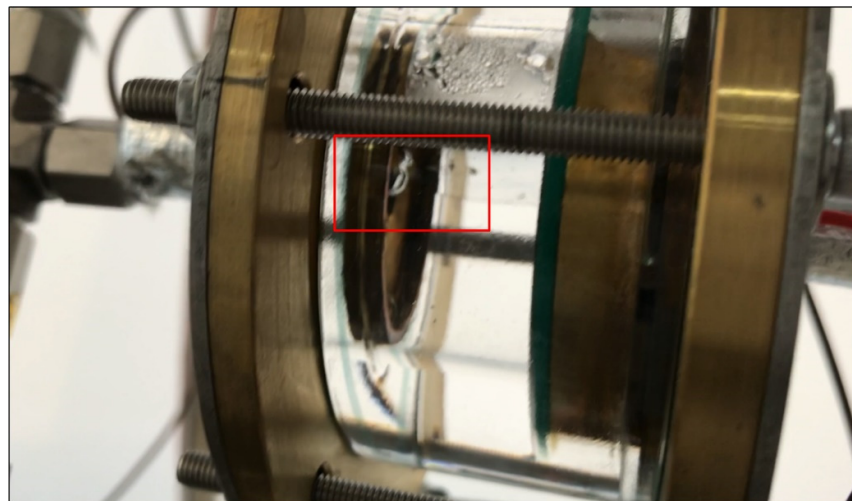


**Figure 14.** Liquid and vapor behavior under an orientation of  $\varphi = -90^\circ$  at a heat load of 105 W (with return liquid).

As the heat load continued to increase to a sufficiently high level ( $\geq 135$  W), the increase in flow resistance resulted in gravity being too insufficient to provide the driving force required for circulation; then, the capillary force began to participate, at which point the FLHP operation switched to a capillarity-gravity co-driven mode. The working fluid in the vapor line was no longer in a two-phase state but was in a pure vapor one (as shown in Figure 15); the evaporator outlet began to show significant superheating.

When the FLHP was operated under an orientation of  $\varphi = -90^\circ$ , no vapor penetration was observed within the test heat load range, which indicated that the heat leak between the

evaporator and the CC was mainly accomplished by the heat conduction of the saturated wick. This might be thanks to the driving effect of gravity, which greatly reduced the pressure difference between the two sides of the vapor-liquid interface inside the capillary wick; the capillary force could play a good gas blocking and sealing effect.

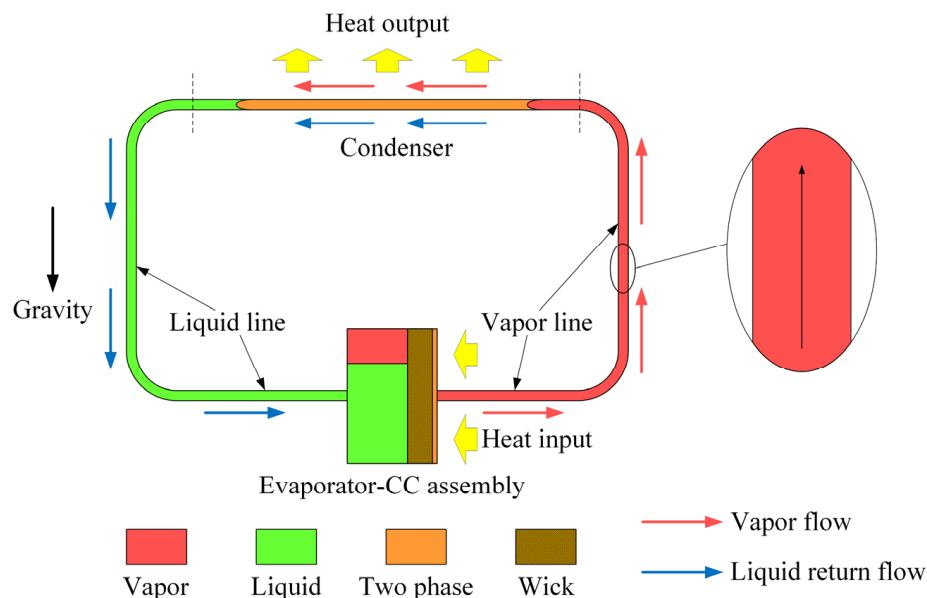


Figure 15. Working fluid distribution and circulation path for capillarity-gravity co-driven mode.

#### 4. Conclusions

In this work, the performances of a disk-shaped evaporator FLHP under three different orientations were investigated; at the same time, the liquid and vapor behaviors in the evaporator-CC assembly were also observed directly. These research results could be helpful in promoting the terrestrial application of FLHPs. Based on the experimental results and visual observations, some key conclusions could be drawn as follows:

1. The startup process was the quickest for the FLHP operating under an orientation of  $\varphi = -90^\circ$ . However, there could be a slight temperature overshoot, resulting in an unsmoothed startup process; the startup speeds under orientations of  $\varphi = 0^\circ$  and  $\varphi = +90^\circ$  were similar, both operating without a significant temperature overshoot;
2. The FLHP orientation could significantly change the heat leak and, therefore, the operating temperature and the heat-transfer limit. Regarding the  $\varphi = +90^\circ$  and  $\varphi = -90^\circ$  orientations, the heat-transfer limits were about 71% and 157% of the  $\varphi = 0^\circ$  orientation, respectively;
3. Based on visual observations, for the loop heat pipe operating in gravity-driven mode, there could be two different paths for the working fluid to return to the evaporator, namely, along the vapor line for low heat loads and along the condenser and liquid lines for relatively large heat loads, respectively.

In terms of the future outlook, this study could be extended by considering more orientations to enrich the understanding of the mechanisms. At the same time, thermal imaging technology and numerical simulation methods could be introduced to compensate for the lack of temperature-distribution measurements in the evaporator and CC.

**Author Contributions:** Conceptualization, X.S. and G.L.; methodology, X.S. and H.W.; validation, Y.L. and H.W.; formal analysis, Y.L. and H.W.; investigation, Y.L. and H.W.; resources, G.L.; data curation, G.L. and Y.G.; writing—original draft preparation, H.W.; writing—review and editing, X.S. and G.L.; visualization, Y.L. and H.W.; supervision, X.S. and G.L.; project administration, G.L.; funding acquisition, G.L. and Y.G. All authors have read and agreed to the published version of the manuscript.

**Funding:** This research was funded by the National Natural Science Foundation of China (No. 52106067 and No. 51576010).

**Data Availability Statement:** The data presented in this study are available on request from the corresponding author. The data are not publicly available due to privacy restrictions.

**Conflicts of Interest:** The authors declare no conflict of interest.

## References

1. Ahmed Qureshi, Z.; Addin Burhan Al-Omari, S.; Elnajjar, E.; Al-Ketan, O.; Abu Al-Rub, R. Architected Lattices Embedded with Phase Change Materials for Thermal Management of High-Power Electronics: A Numerical Study. *Appl. Therm. Eng.* **2023**, *219*, 119420. [\[CrossRef\]](#)
2. Al-Omari, S.A.B.; Qureshi, Z.A.; Elnajjar, E.; Mahmoud, F. A Heat Sink Integrating Fins within High Thermal Conductivity Phase Change Material to Cool High Heat-Flux Heat Sources. *Int. J. Therm. Sci.* **2022**, *172*, 107190. [\[CrossRef\]](#)
3. Du, K.; Calautit, J.; Wang, Z.; Wu, Y.; Liu, H. A Review of the Applications of Phase Change Materials in Cooling, Heating and Power Generation in Different Temperature Ranges. *Appl. Energy* **2018**, *220*, 242–273. [\[CrossRef\]](#)
4. Kadam, S.T.; Kumar, R. Twenty First Century Cooling Solution: Microchannel Heat Sinks. *Int. J. Therm. Sci.* **2014**, *85*, 73–92. [\[CrossRef\]](#)
5. Hassan, I.; Phutthavong, P.; Abdelgawad, M. Microchannel Heat Sinks: An Overview of the State-of-the-Art. *Microscale Thermophys. Eng.* **2004**, *8*, 183–205. [\[CrossRef\]](#)
6. Khandekar, S.; Sahu, G.; Muralidhar, K.; Gatapova, E.Y.; Kabov, O.A.; Hu, R.; Luo, X.; Zhao, L. Cooling of High-Power LEDs by Liquid Sprays: Challenges and Prospects. *Appl. Therm. Eng.* **2021**, *184*, 115640. [\[CrossRef\]](#)
7. Smakulski, P.; Pietrowicz, S. A Review of the Capabilities of High Heat Flux Removal by Porous Materials, Microchannels and Spray Cooling Techniques. *Appl. Therm. Eng.* **2016**, *104*, 636–646. [\[CrossRef\]](#)
8. Kandlikar, S.G.; Bapat, A.V. Evaluation of Jet Impingement, Spray and Microchannel Chip Cooling Options for High Heat Flux Removal. *Heat Transfer. Eng.* **2007**, *28*, 911–923. [\[CrossRef\]](#)
9. Kim, J. Spray Cooling Heat Transfer: The State of the Art. *Int. J. Heat Fluid Flow* **2007**, *28*, 753–767. [\[CrossRef\]](#)
10. Xiong, K.; Meng, L.; Wang, S.; Zhang, L.W. Experimental Investigation on Thermal Characteristics of a Novel Loop Heat Pipe for Cooling High Heat Flux Electronic Chips. *Int. J. Heat Mass Transf.* **2022**, *187*, 122569. [\[CrossRef\]](#)
11. Hoang, T.T.; O’Connell, T.A.; Ku, J.; Dan Butler, C.; Swanson, T.D. Miniature Loop Heat Pipes for Electronic Cooling. In Proceedings of the Advanced Electronic Packaging, Maui, HI, USA, 6–11 July 2003; American Society of Mechanical Engineers: New York, NY, USA, 2003; Volume 2, pp. 517–525.
12. Vasiliev, L.; Lossouarn, D.; Romestant, C.; Alexandre, A.; Bertin, Y.; Piatsiushyk, Y.; Romanenkov, V. Loop Heat Pipe for Cooling of High-Power Electronic Components. *Int. J. Heat Mass Transf.* **2009**, *52*, 301–308. [\[CrossRef\]](#)
13. Maydanik, Y.F. Loop Heat Pipes. *Appl. Therm. Eng.* **2005**, *25*, 635–657. [\[CrossRef\]](#)
14. Maydanik, Y.F.; Vershinin, S.V.; Chernysheva, M.A. Experimental Study of an Ammonia Loop Heat Pipe with a Flat Disk-Shaped Evaporator Using a Bimetal Wall. *Appl. Therm. Eng.* **2017**, *126*, 643–652. [\[CrossRef\]](#)
15. Maydanik, Y.F.; Vershinin, S.V.; Chernysheva, M.A. The Results of Comparative Analysis and Tests of Ammonia Loop Heat Pipes with Cylindrical and Flat Evaporators. *Appl. Therm. Eng.* **2018**, *144*, 479–487. [\[CrossRef\]](#)
16. Launay, S.; Sartre, V.; Bonjour, J. Parametric Analysis of Loop Heat Pipe Operation: A Literature Review. *Int. J. Therm. Sci.* **2007**, *46*, 621–636. [\[CrossRef\]](#)
17. Maydanik, Y.F.; Chernysheva, M.A.; Pastukhov, V.G. Review: Loop Heat Pipes with Flat Evaporators. *Appl. Therm. Eng.* **2014**, *67*, 294–307. [\[CrossRef\]](#)
18. Celata, G.P.; Cumo, M.; Furrer, M. Experimental Tests of a Stainless Steel Loop Heat Pipe with Flat Evaporator. *Exp. Therm. Fluid Sci.* **2010**, *34*, 866–878. [\[CrossRef\]](#)
19. Chen, B.-B.; Liu, W.; Liu, Z.-C.; Yang, J.-G.; Li, H. Experimental Study on Miniature Loop Heat Pipe with Flat-Plate Evaporator. *J. Astronaut.* **2011**, *32*, 953–958. [\[CrossRef\]](#)
20. Wu, T.; Wang, T.; Ma, Z.; Zhang, Z.; Liu, W.; Liu, Z. Experimental Investigation on the Start-up Performance of a Loop Heat Pipe with Three Flat Disk Evaporators Combined. *Appl. Therm. Eng.* **2022**, *216*, 119128. [\[CrossRef\]](#)
21. Cimbala, J.M.; Brenizer, J.S., Jr.; Chuang, A.P.-Y.; Hanna, S.; Conroy, C.T.; El-Ganayni, A.A.; Riley, D.R. Study of a Loop Heat Pipe Using Neutron Radiography. *Appl. Radiat. Isot.* **2004**, *61*, 701–705. [\[CrossRef\]](#)
22. Chuang, P.-Y.A.; Cimbala, J.M.; Brenizer, J.S. Experimental and Analytical Study of a Loop Heat Pipe at a Positive Elevation Using Neutron Radiography. *Int. J. Therm. Sci.* **2014**, *77*, 84–95. [\[CrossRef\]](#)
23. Chuang, P.-Y.A.; Cimbala, J.M.; Brenizer, J.S., Jr.; Conroy, C.T. Theoretical and Experimental Study of a Loop Heat Pipe at Positive Elevation. In Proceedings of the ASME 2004 International Mechanical Engineering Congress and Exposition, Anaheim, CA, USA, 13–19 November 2004; Volume 375, pp. 67–74.
24. Okamoto, A.; Hatakenaka, R.; Mase, Y.; Murakami, M. Visualization of a Loop Heat Pipe Using Neutron Radiography. In Proceedings of the 40th International Conference on Environmental Systems, Barcelona, Spain, 11–15 July 2010.

25. Hatakenaka, R.; Okamoto, A.; Mase, Y.; Murakami, M.; Iikura, H. Visualization of Internal Fluid Behavior in a Miniature Loop Heat Pipe Using Neutron Radiography. In Proceedings of the 41st International Conference on Environmental Systems, Portland, OR, USA, 17–21 July 2011.
26. Maydanik, Y.F.; Pastukhov, V.G.; Kichanov, S.E. Visual Studies of the Operation of Loop Heat Pipes by Neutron Radiography. *Therm. Sci. Eng. Prog.* **2022**, *35*, 101444. [[CrossRef](#)]
27. D'Entremont, B.P.; Ochterbeck, J.M. Investigation of Loop Heat Pipe Startup Using Liquid Core Visualization. In Proceedings of the ASME 2008 Heat Transfer Summer Conference collocated with the Fluids Engineering, Energy Sustainability, and 3rd Energy Nanotechnology Conferences, Jacksonville, FL, USA, 10–14 August 2008; American Society of Mechanical Engineers: New York, NY, USA, 2009; Volume 2, pp. 387–393.
28. D'Entremont, B.P.; Ochterbeck, J.M. Performance of Low-Conductivity Ceramic Wicks in Capillary Evaporators. In Proceedings of the 40th Thermophysics Conference, Seattle, WA, USA, 23–26 June 2008.
29. Chang, X.; Watanabe, N.; Nagai, H.; Nagano, H. Visualization of Thermo-Fluid Behavior of Loop Heat Pipe with Two Evaporators and One Condenser under Various Orientation with Even Heat Loads. *Int. J. Heat Mass Transf.* **2022**, *198*, 123397. [[CrossRef](#)]
30. Chang, X.; Watanabe, N.; Nagano, H. Visualization Study of a Loop Heat Pipe with Two Evaporators and One Condenser under Gravity-Assisted Condition. *Int. J. Heat Mass Transf.* **2019**, *135*, 378–391. [[CrossRef](#)]
31. Gunnasegaran, P.; Abdullah, M.Z.; Shuaib, N.H. Influence of Nanofluid on Heat Transfer in a Loop Heat Pipe. *Int. Commun. Heat Mass Transf.* **2013**, *47*, 82–91. [[CrossRef](#)]
32. Yan, K.; Xie, R.; Li, N.; Xu, G.; Wu, Y. Experimental Investigation and Visualization Study of the Condensation Characteristics in a Propylene Loop Heat Pipe. *J. Therm. Sci.* **2021**, *30*, 1803–1813. [[CrossRef](#)]
33. Li, X.; Zhang, Z.; Wang, Y.; Zhu, K.; Liu, S. Characteristic of Temperature Oscillation during the Operation of Loop Heat Pipe Enhanced by Pressure Head of Evaporation. *Heat Mass Transf.* **2022**, *58*, 1145–1155. [[CrossRef](#)]
34. Shao, B.; Jiang, Z.; Xu, G.; Liu, L.; Li, N.; Dong, D. Numerical and Experimental Study on the Vapor-Liquid Distribution of Loop Heat Pipe with Varying Density of Working Fluid. *Appl. Therm. Eng.* **2023**, *226*, 120278. [[CrossRef](#)]
35. Qu, Y.; Cheng, L.; Luan, T. Manufacture and Performance Simulation of a Visible Miniature Loop Heat Pipe. In Proceedings of the 2007 First International Conference on Integration and Commercialization of Micro and Nanosystems, Hainan, China, 10–13 January 2007; Volume A, pp. 777–784.
36. Lin, G.; Li, N.; Bai, L.; Wen, D. Experimental Investigation of a Dual Compensation Chamber Loop Heat Pipe. *Int. J. Heat Mass Transf.* **2010**, *53*, 3231–3240. [[CrossRef](#)]
37. Nishikawara, M.; Otani, K.; Ueda, Y.; Yanada, H. Liquid–Vapor Phase Behavior and Operating Characteristics of the Capillary Evaporator of a Loop Heat Pipe at Start-Up. *Int. J. Therm. Sci.* **2018**, *129*, 426–433. [[CrossRef](#)]
38. Nishikawara, M.; Ueda, Y.; Yanada, H. Static and Dynamic Liquid-Vapor Phase Distribution in the Capillary Evaporator of a Loop Heat Pipe. *Microgravity Sci. Technol.* **2019**, *31*, 61–71. [[CrossRef](#)]
39. Zhang, Q.; Lin, G.; Shen, X.; Bai, L.; Wen, D. Visualization Study on the Heat and Mass Transfer in the Evaporator-Compensation Chamber of a Loop Heat Pipe. *Appl. Therm. Eng.* **2020**, *164*, 114472. [[CrossRef](#)]
40. Takamatsu, T.; Hisano, K.; Iwasaki, H. Improvement of Heat Transfer Performance of Loop Heat Pipe for Electronic Devices. In Proceedings of the ASME 2011 Pacific Rim Technical Conference and Exhibition on Packaging and Integration of Electronic and Photonic Systems, Portland, OR, USA, 6–8 July 2011; Volume 2, pp. 165–172.
41. Bartuli, E.; Vershinin, S.; Maydanik, Y. Visual and Instrumental Investigations of a Copper-Water Loop Heat Pipe. *Int. J. Heat Mass Transf.* **2013**, *61*, 35–40. [[CrossRef](#)]
42. Zhou, G.; Li, J. Two-Phase Flow Characteristics of a High Performance Loop Heat Pipe with Flat Evaporator under Gravity. *Int. J. Heat Mass Transf.* **2018**, *117*, 1063–1074. [[CrossRef](#)]
43. Wang, X.; Yang, J.; Wen, Q.; Shittu, S.; Liu, G.; Qiu, Z.; Zhao, X.; Wang, Z. Visualization Study of a Flat Confined Loop Heat Pipe for Electronic Devices Cooling. *Appl. Energy* **2022**, *322*, 119451. [[CrossRef](#)]
44. Du, S.; Zhang, Q.; Ling, L.; Zou, S.; Liu, L.; Meng, F. Visualization Investigation on Temperature Oscillation and Two-Phase Behaviors of A Flat Loop Heat Pipe. *J. Therm. Sci.* **2023**. [[CrossRef](#)]
45. Mo, D.; Zou, G.; Lu, S.; Winston Zhang, L. A Flow Visualization Study on the Temperature Oscillations inside a Loop Heat Pipe with Flat Evaporator. In *International Electronic Packaging Technical Conference and Exhibition*; American Society of Mechanical Engineers (ASME): New York, NY, USA, 2013; Volume 55768, p. V002T08A037.
46. Anand, A.R.; Jaiswal, A.; Ambirajan, A.; Dutta, P. Experimental Studies on a Miniature Loop Heat Pipe with Flat Evaporator with Various Working Fluids. *Appl. Therm. Eng.* **2018**, *144*, 495–503. [[CrossRef](#)]
47. Xu, J.; Zhang, L.; Xu, H.; Zhong, J.; Xuan, J. Experimental Investigation and Visual Observation of Loop Heat Pipes with Two-Layer Composite Wicks. *Int. J. Heat Mass Transf.* **2014**, *72*, 378–387. [[CrossRef](#)]
48. Xu, J.; Wang, Z.; Xu, H.; Zhang, L. Experimental Research on the Heat Performance of a Flat Copper-Water Loop Heat Pipe with Different Inventories. *Exp. Therm. Fluid Sci.* **2017**, *84*, 110–119. [[CrossRef](#)]
49. Zhao, S.C.; Zhang, Z.K.; Zhao, R.Z.; Liu, Z.C.; Liu, W. Experimental Study on Global Visualization of Loop Heat Pipe with a Flat Disk-Shaped Evaporator. *Energy Rep.* **2022**, *8*, 10895–10912. [[CrossRef](#)]
50. Chuang, P.-Y.A.; Cimbalá, J.M.; Brenizer, J.S., Jr.; Conroy, C.T. Analytical Modeling of a Loop Heat Pipe at Positive Elevation. In Proceedings of the ASME 2004 International Mechanical Engineering Congress and Exposition, Anaheim, CA, USA, 13–19 November 2004; American Society of Mechanical Engineers (ASME): New York, NY, USA, 2004; Volume 375, pp. 629–635.

51. Wang, H.; Lin, G.; Shen, X.; Bai, L.; Yang, R.; Wen, D. Effect of Evaporator/Condenser Elevations on a Loop Heat Pipe with Non-Condensable Gas. *Appl. Therm. Eng.* **2020**, *180*, 115711. [[CrossRef](#)]
52. Bai, L.; Guo, J.; Lin, G.; He, J.; Wen, D. Steady-State Modeling and Analysis of a Loop Heat Pipe under Gravity-Assisted Operation. *Appl. Therm. Eng.* **2015**, *83*, 88–97. [[CrossRef](#)]
53. Tuhin, A.R.; Huynh, P.H.; Htoo, K.Z.; Kariya, K.; Miyara, A. Thermal Performance Comparison of Flat Plate Evaporator Loop Heat Pipe Operating between Horizontal Condition and Gravity Assisted Condition. *J. Phys. Conf. Ser.* **2018**, *1086*, 012013. [[CrossRef](#)]
54. Li, C.; Liu, Z.; Zhang, X. Steady-State Operating Characteristics Analysis of Loop Heat Pipes with Flat-Plate Evaporator. *Therm. Sci. Eng. Prog.* **2022**, *28*, 101070. [[CrossRef](#)]

**Disclaimer/Publisher's Note:** The statements, opinions and data contained in all publications are solely those of the individual author(s) and contributor(s) and not of MDPI and/or the editor(s). MDPI and/or the editor(s) disclaim responsibility for any injury to people or property resulting from any ideas, methods, instructions or products referred to in the content.